Int. J. Microgravity Sci. Appl. **33**(1) (2016) 33110
DOI: 10.15011/jasma.33.33110

||||| Original Paper |||||

Splash and Bounce of Droplet on Liquid Layer under Low-Gravity

Suguru SHIRATORI [1], Shumpei OZAWA [1, 2] and Taketoshi HIBIYA [1, 3]

Abstract

Fluid motions after an impact of a droplet on a thin liquid layer were investigated by experimental observation under low gravity condition using the parabolic flight of an airplane. Whether the droplet bounces or coalesces on the liquid layer was found to be dependent on the Weber number and also on the Bond number, which represents the relative importance of gravity. In the plane of the Weber and the Bond numbers, droplet bouncing occurred for larger Weber numbers when the Bond number was small. The appearance of secondary droplets, which are caused by a symmetry-breaking of the growing cylindrical liquid sheet, was found to be independent to gravity. Our experimental results do not find gravity-dependent instability to be a cause of the symmetry-breaking, because it was observed even under microgravity conditions.

Keyword(s): Droplet impact, Mode selection, Rayleigh-Plateau, Weber number, Bond number, Bounce, Splash, Parabolic flight
Received 5 November 2015; Accepted 14 January 2016; Published 31 January 2016

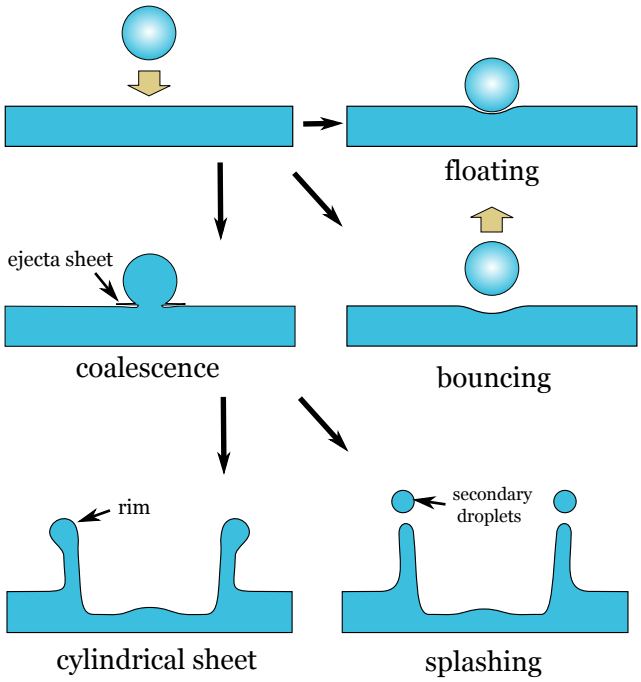

Fig. 1 Morphology classification of a droplet impact on a liquid layer.

1. Introduction

The splashing of droplets on a liquid layer or a dry surface can be observed in daily life and many industrial situation such as liquid droplet radiators [1)], ink jet printers [2)], direct injection engines [3)], and so on. Worthington [4,5)] was a pioneer who took many photographs of splashes using electrical spark illumination. After his investigation, many experimental and numerical studies have been carried out on this phenomenon, as systematically reviewed by Yarin [6)]. Recently, splashing phenomena even for metallic melts have been studied numerically by Tagawa [7)] and experimentally by Li et al. [8)]. The fluid motion after the impact strongly depends on the velocity of the impact and the size of the droplet. Besides these parameters, the phenomenon shows variations depending on the physical properties of the liquid droplet and also on the type of surface, which may be a dry solid substrate, a deep pool, or a thin liquid layer. Even on a thin liquid layer, to which we shall confine the discussion in the following, the droplet impact shows various morphology, such as floating, bouncing, coalescence and splashing [9)], as shown in **Fig. 1**. More detailed classifications have been provided (e.g. Deegan et al. [10)]).

These varieties and the occurrence conditions of the fluid motion have been investigated using nondimensional Weber, Reynolds, Bond, and Ohnesorge numbers, defined as follows:

$$We = \frac{\rho U^2 D}{\sigma}, \tag{1a}$$

$$Re = \frac{\rho U D}{\mu}, \tag{1b}$$

$$Bo = \frac{\rho g D^2}{\sigma}, \tag{1c}$$

$$Oh = \frac{\mu}{\sqrt{\rho \sigma D}} = \frac{\sqrt{We}}{Re}, \tag{1d}$$

where ρ, σ, and μ are the density, the surface tension, and the viscosity of the fluid, respectively. D is the diameter of the droplet,

1 Department of Aerospace System Engineering, Tokyo Metropolitan University, 6-6, Asahigaoka, Hino 191-0065, Japan.
2 Department of Mechanical Science and Engineering, Chiba Institute of Technology, 2-17-1, Tsudanuma, Narashino 275-0016, Japan.
3 Graduate School of System Design and Management, Keio University, 1-1, Hiyoshi 4-chome, Kohoku-ku, Yokohama 223-8526, Japan.
(E-mail: shumpei.ozawa@it-chiba.ac.jp)

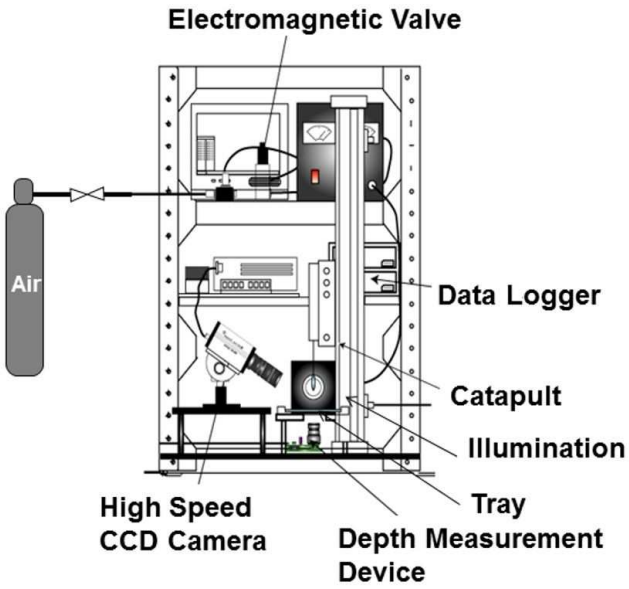

Fig. 2 Schematic of experimental apparatus for use under microgravity and terrestrial conditions.

U denotes the impact velocity, and g is the gravitational acceleration. When the impact energy of the droplet is sufficiently low, the droplet bounces from the liquid layer. Gopinath & Koch [11] have suggested an explanation for the mechanism of this bouncing, in terms of an air gap between droplet-layer surfaces. Because of the restorable surface deformation of both the droplet and the layer, the air gap inhibits the coalescence of those surfaces. When the impact energy of the droplet increases, the air gap can no more be sustained and the droplet coalesces to the liquid layer. The condition for the appearance of bouncing has been investigated, in terms of the Weber number We and the Ohnesorge number Oh [12,13]. The upper bound of Weber number for bouncing was reported as We = 10-50 for the range of Ohnesorge number $Oh < 5 \times 10^{-2}$. In their papers, the dependence of the Bond number on the bouncing threshold, which is one of the issues in this paper, is not mentioned. The bouncing of the droplet is also investigated for the cases that the surface is restricted by a cylindrical wall [14], or that the surface is vibrated [15].

In the context of the coalescence of the droplet and the liquid layer, researchers have been attracted by phenomena appearing immediately after the coalescence, including the so-called ejecta sheet [16,17], the air-entrainment and its rupture [12], and formation of micro-bubbles [13]. Since Zhang et al. [16] introduced novel X-ray visualization, details of the early stage of the ejecta sheet formation have become clarified. After the early stage of the coalescence, a cylindrical liquid sheet forms from the layer, extending upward and outward with a torus-like rim forming along the brim of the sheet. The formation of this sheet has been modeled by Peregrine [18]. The rim then loses its axi-symmetry due to an instability, which causes an azimuthal variation in the rim thickness. This thickness variation develops and results in a crown-like shape, which may break into secondary droplets (also called a coronet). Two different interpretations have been suggested for the formation mechanism of these secondary droplets; by Rayleigh-Taylor instability [19] and by Rayleigh-Plateau instability [20]. Deegan et al. [10] and Zhang et al. [21] carefully observed droplet impacts and classified their qualitative features into four categories in the plane of the Weber number We and the Reynolds number Re. Their classification is based on whether the Peregrine's sheet is disordered or not. For larger Reynolds numbers, Peregrine's sheet is prone to be disturbed, which makes splashes more complicated. Zhang et al. [21] considered the instability mechanism from the aspect of a wavelength selection of the crown splashes, and concluded that the Rayleigh-Plateau instability is essential.

The effects of gravity on the droplet impact, which is the focus of this paper, have not been regarded as important in almost all the previous discussions [6]. Generally in fluid physics, the effect of gravity is often characterized by the Bond number Bo, which is interpreted as the ratio of the square of the characteristic length of the system, which corresponds to D here, to the square of the capillary length;

$$L_c = \sqrt{\frac{\sigma}{\rho g}}. \tag{2}$$

On the ground, where gravitational acceleration is constant, it is impossible to change the Bond number independently of other parameters listed in Eq. (1), because the droplet diameter D is the sole component by which to change the Bond number for the same liquid. This would be the reason why attention has not been paid to the effect of gravity.

A microgravity environment is a direct way to change the Bond number of the system. On board the International Space Station, where the gravitational acceleration is as small as 10^{-4} G, the NASA astronaut Pettit observed the bouncing and coalescence of a water droplet on the inner surface of a hollow water shell [22]. In his experiment, the water droplet seems to bounce easily even for fast impact cases, although detailed parameters have not been provided. From his experiment, we are motivated to investigate the gravity-dependence of droplet bouncing. This paper aims to clarify the effects of gravity on droplet impact phenomena, in particular on bouncing/splashing outcome and secondary droplet formation. Experiments were carried out both on earth and under microgravity obtained through the parabolic flight of an airplane.

After the experimental setup is described in Sec. 2, the results are summarized in Sec. 3. The discussion is provided in Sec. 4, which precedes our conclusion in Sec. 5.

2. Experimental setup

Figure 2 shows a schematic of the experimental apparatus for use in experiments under microgravity and terrestrial conditions.

Table 1 Physical properties of the liquids employed at 25℃.

Symbol	Meaning	Unit	Silicone oil[23)]	Water
ρ	Density	$\mathrm{kg{\cdot}m^{-3}}$	925	1000
ν	Kinematic viscosity	$10^{-6}\mathrm{m^2{\cdot}s^{-1}}$	6	1
μ	Dynamic viscosity	$10^{-3}\mathrm{Pa{\cdot}s}$	5.55	1
σ	Surface tension	$10^{-3}\mathrm{N{\cdot}m^{-1}}$	19.8	70.0

Table 2 Nomenclature of experimental parameters and their ranges of value realized in the present work.

Symbol		Meaning	Unit	Range of value
D		Droplet diameter	10^{-3}m	$1.1 \sim 4.4$
U		Impact velocity	$\mathrm{m{\cdot}s^{-1}}$	$0.5 \sim 2.3$
H		Thickness of liquid layer	10^{-3}m	$1 \sim 2$
g		Gravitational acceleration	$\mathrm{m{\cdot}s^{-2}}$	2×10^{-2}G, 0.2G, and 1G
G		g on earth	$\mathrm{m{\cdot}s^{-2}}$	9.81
Bo	$=\rho g D^2/\sigma$	Bond number	—	$1.6\times10^{-3} \sim 4.1$
We	$=\rho U^2 D/\sigma$	Weber number	—	$18 \sim 1018$
Re	$=\rho U D/\mu$	Reynolds number	—	$213 \sim 1799$
Oh	$=\mu/(\rho\sigma D)^{-1/2}$	Ohnesorge number	—	$1.6\times10^{-2} \sim 2.9\times10^{-2}$

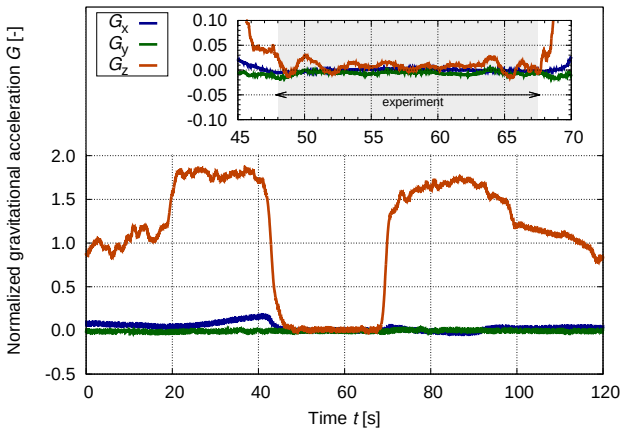

Fig. 3 Typical time evolution of the gravity acceleration normalized by its terrestrial value. The experimental observations are carried out within the time range from 48.0 to 67.5s. The directions x and z are oriented to the traveling and the height-wise direction, respectively. In this case the averages of the gravity during the experiment are $\overline{g_x} = -5.4\times10^{-4}$G, $\overline{g_y} = -6.5\times10^{-3}$G, and $\overline{g_z} = 8.8\times10^{-3}$G, respectively, whereas the standard deviations are $s_x = 2.5\times10^{-3}$G, $s_y = 3.5\times10^{-3}$G, and $s_z = 1.0\times10^{-2}$G, respectively.

The apparatus consists of a catapult for droplet formation driven by an air cylinder, a tray for sustaining a liquid film, a high-speed video (HSV) camera (Redlake Motion Scope PCI), a halogen lamp illumination, a laptop PC, and a data logger (Keyence NR-1000). Silicone oil and water were used as liquids for droplets and layers. Their physical properties are listed in **Table 1**.

On the ground, the impact velocity of the droplet on the layer can be easily controlled by adjusting the initial height of the droplet. In contrast, under low-gravity condition, the droplet must be given a sufficient initial velocity to make a collision. The initial velocity is given by an air-cylinder-driven catapult, and the values achieved in our experiments were within the range of 0.5 to 2.3 $\mathrm{m{\cdot}s^{-1}}$. The fluid motion around the moment of the droplet impact was recorded by the HSV at a frame rate of 500 fps.

During a parabolic flight, the gravitational acceleration g was varied from 2×10^{-2} to 0.2 G, by controlling the pitch angle of the airplane Gulfstream-II operated by Diamond Air Service Inc. (Aichi, Japan). A typical time-line of the gravity is shown in **Fig. 3**. The directions x and z are oriented to the traveling and the height-wise direction, respectively. In this case, the experimental observations were carried out within the time range from 48.0 to 67.5s. In this case the averages of the gravity during the experiment are $\overline{g_x} = -5.4\times10^{-4}$G, $\overline{g_y} = -6.5\times10^{-3}$G, and $\overline{g_z} = 8.8\times10^{-3}$G, respectively, whereas the standard deviations are $s_x = 2.5\times10^{-3}$G, $s_y = 3.5\times10^{-3}$G, and $s_z = 1.0\times10^{-2}$G, respectively.

The liquid layer was formed by supplying the liquid in a square tray of 150×150 mm size. Under the low-gravity condition, the liquid layer may rise up the wall of the tray by a wettability. In order to prevent this rising-up, the oil-repellent coating was partially applied on the inside wall of the tray, remaining a desired height for the layer. The height of the liquid layer can roughly be estimated by counting the dispensed liquid volume, although, in practice, the height cannot be kept constant due to the lateral acceleration. In the beginning of the each sequence of parabolic flight, the gravity in the traveling direction g_x increases due to the posture of the plane. In the case shown in **Fig. 3**, g_x increases up to 0.1G before the height-wise gravity g_z steeply decreases. Such a lateral gravity affects as similar to the inclining of the tray,

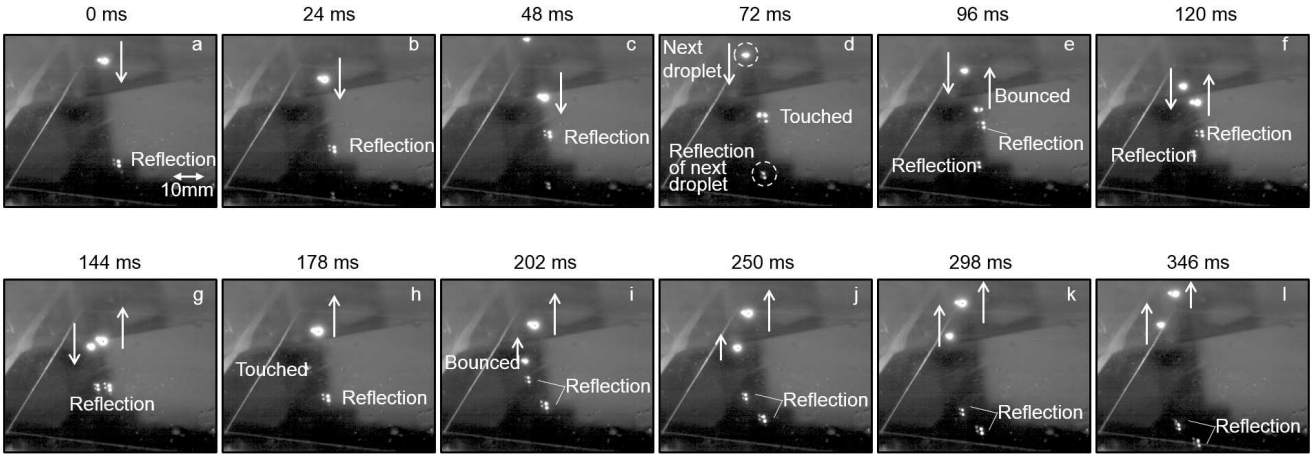

Fig. 4 Selected snapshots indicating the bouncing of silicone oil droplets under 2×10^{-2} G condition. The elapsed time counting from the first (upper-left) picture is shown at the top of each picture. The impact velocity U and the diameter D are calculated as U = 0.36 m·s^{-1} and D = 6.4 $\times 10^{-3}$ m and U = 0.31 m·s^{-1} and D = 4.1 $\times 10^{-3}$ m for the former droplet and the latter droplet, respectively. The nondimensional parameters are calculated as: We = 39.2, Re = 385, and Bo = 3.71$\times 10^{-1}$ for the former droplet, and We = 18.6, Re = 214, and Bo = 1.57$\times 10^{-1}$ for the latter droplet. (Movie) an embedded movie can be played with an external player by clicking the icon shown near the figure. The movie is recorded at a frame rate of 500 fps, whereas the playing speed in the movie file is slowed down to 30 fps.

and it causes the thickness undulation of the liquid layer. In the context of the lubrication theory, the time constant for the gravity leveling can be estimated as $\tau = \nu\lambda^2/(gH^3)$, where λ denotes the lateral length scale of the deformation. In the present experiment τ is estimated as 140 s, which is much longer than the time period where g_x has significant value (**Fig. 3**). Furthermore, in our experiment, the droplet impacts were observed in the center of the tray as possible. Based on the above mentioned consideration, the layer height realized in our experiments is estimated in the range of 1-2mm.

The experiment was also carried out under the normal gravity condition on earth. The ranges of the realized parameters of the droplet diameter D, the impact velocity U, and the thickness of the layer H throughout all the experiments are summarized in **Table 2**.

3. Results

Figures 4 and **5** show some selected snapshots of typical motions of silicone oil droplets observed under a gravitational level of 2×10^{-2} G and 0.2 G, respectively. **Fig. 6** shows the case for a water droplet under $g = 2 \times 10^{-2}$ G condition. In these figures, both the bouncing and the splashing of the droplet can be recognized, with some help from the reflection image of the flying droplet.

In **Fig. 4**, two droplets are ejected from the upper side, approach the liquid layer, and then bounce on the surface. Bouncing was recognized at 72 ms (**Fig. 4**d) and 178 ms (**Fig. 4**h). In **Fig. 5**, the motion of two adjacent small droplets can be observed. The first droplet splashes at 20 ms, whereas the latter droplet shows repetitive bouncing (**Fig. 5**e-k). Finally the latter droplet stayed on the surface for a time period of 90 ms (**Fig. 5**k) and then coalesced with the pool of silicone oil (**Fig. 5**l). For the water droplet, bouncing was also observed under the 2×10^{-2} G condition, as shown in **Fig. 6**.

Whether the droplet bounces or splashes depends on conditions such as the impact velocity and the droplet size. The smaller the diameter and the velocity, the more easily bouncing was observed. Furthermore, the mode selection was also affected by the gravitational acceleration. Under our experimental conditions, bouncing took place more than splashing under the gravitational condition of 2×10^{-2} G, whereas under the normal gravity condition on earth bouncing was not observed. **Fig. 7** summarizes all the experiments in the plane of the Weber and Bond numbers, with respect to whether splashing or bouncing is observed. The droplet appears to bounce under condition of a lower Weber number or lower Bond number. This would be the first investigation which suggests the bouncing/splashing boundary to be along such a wide range of Bond number. For the case of the water droplet, our experiment was performed only under the condition of $g = 2 \times 10^{-2}$ G, and all the observed impacts resulted in bouncing. The calculated We and Bo for the case of water are significantly smaller than those for silicone oil, since realized impact velocities U are small, and the surface tension σ of water is relatively large (see **Table 1**).

The results are also summarized from the viewpoint of the axi-symmetry of splashing. When the splashing took place, a growing liquid column loses its axi-symmetry followed by the breakup to secondary droplets, as shown in **Fig. 8**. The occurrence of the

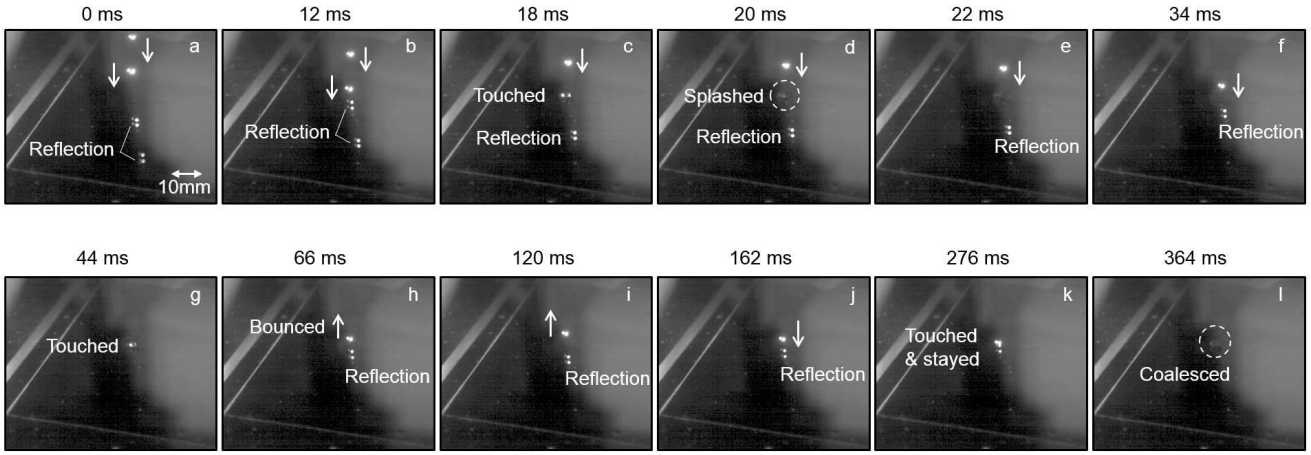

Fig. 5 Selected snapshots indicating the bouncing and splashing of silicone oil droplets under 0.2 G condition. The elapsed time counting from the first (upper-left) picture is shown at the top of each picture. The impact velocity U and the diameter D are calculated as $U = 0.61$ m·s^{-1} and $D = 4.4 \times 10^{-3}$ m, and; $U = 0.59$ m·s^{-1} and $D = 3.8 \times 10^{-3}$ m for the former (bouncing) droplet and the latter droplet, respectively. The nondimensional parameters are calculated as: $We = 74.4$, $Re = 439$, and $Bo = 1.73$ for the former droplet, and $We = 61.3$, $Re = 373$, and $Bo = 1.33$ for the latter droplet. (Movie) an embedded movie can be played with an external player by clicking the icon shown near the figure. The movie is recorded at a frame rate of 500 fps, whereas the playing speed in the movie file is slowed down to 30 fps.

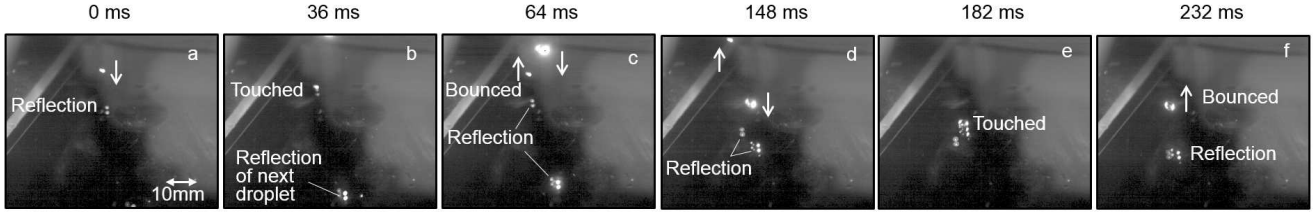

Fig. 6 Selected snapshots indicating the bouncing of water droplets under 2×10^{-2} G condition. The elapsed time counting from the first (left) picture is shown at the top of each picture. The impact velocity U and the diameter D are calculated as $U = 0.16$ m·s^{-1} and $D = 2.3 \times 10^{-3}$ m, and $U = 0.20$ m·s^{-1} and $D = 5.1 \times 10^{-3}$ m for the former droplet and the latter droplet, respectively. The nondimensional parameters are calculated as: $We = 0.88$, $Re = 377$, and $Bo = 1.49 \times 10^{-1}$ for the former droplet, and $We = 2.89$, $Re = 1008$, and $Bo = 7.11 \times 10^{-1}$ for the latter droplet. (Movie) an embedded movie can be played with an external player by clicking the icon shown near the figure. The movie is recorded at a frame rate of 500 fps, whereas the playing speed in the movie file is slowed down to 30 fps.

symmetry-breaking is distinguished by a wavenumber of the surface shape along the rim of the liquid columns. **Figure 9** summarizes the Reynolds number Re and the Weber number We realized in the present study. In the figure, the filled symbols correspond to a splash with wavenumber $m > 0$ and the opened symbols to $m = 0$. The appearance of $m > 0$ splashing takes place under the condition of when both Re and We are large. In the figure, the dashed line of $We \cdot Re^{1/2} = 2.6 \times 10^4$ is the threshold condition, which is suggested by Deegan et al.[10] for the occurrence of symmetry-breaking. The line approximately separates our experimental results, albeit with an indistinct threshold, into two regions according to whether the wavenumber is $m = 0$ or $m > 0$.

4. Discussion

Let us discuss the effect of gravity on droplet impact from two points of view; whether the droplet bounces or splashes, and the formation of secondary droplets after the splash. The bounce of droplets has previously been observed by other researchers and its mechanism explained in terms of the existence of an air gap between the droplet and the liquid layer. Gopinath & Koch[11] considered this droplet-layer collision using a spring-mass model, assuming that the surrounding air is incompressible. According to them, a picture of the bouncing process with the droplet-layer interaction can be understood as follows. The initial momentum energy of the approaching droplet is mainly spent in a recoverable surface deformation of both the droplet and the layer, and the droplet loses its velocity. When the air gap thickness becomes a certain value, both the surfaces start to deform, making a dimple

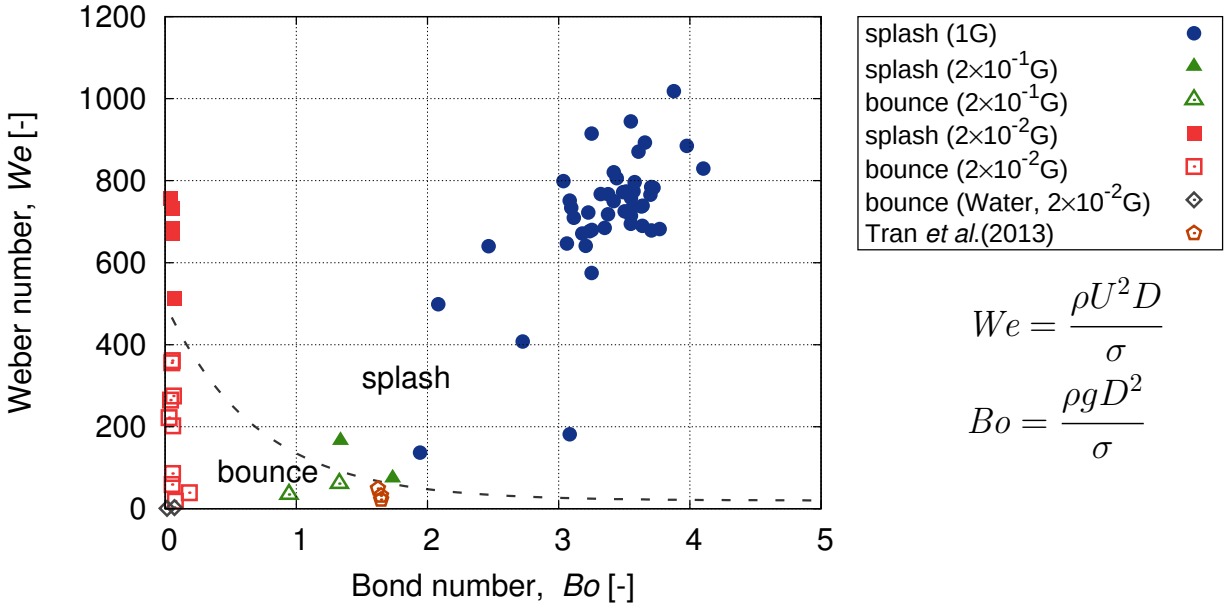

Fig. 7 Mode selection map based on the Weber and Bond numbers. Open symbols stand for cases of bouncing, whereas filled symbols stand for splashing. The symbols ○, △, and □ stand for the different gravity levels 1 G, 0.2 G, and 2×10^{-2} G, respectively. The pentagon symbols are the results of Tran et al. [12]. The dashed line stands for an eye-guide.

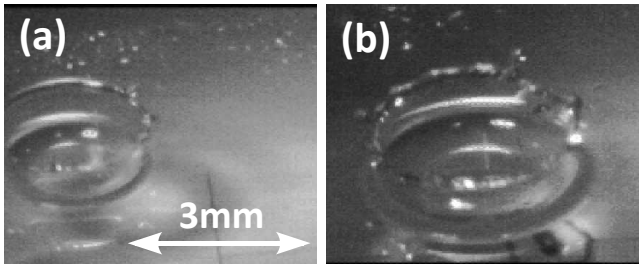

Fig. 8 Splashing of the silicone oil droplets under microgravity (2×10^{-2} G). (a) Axisymmetric splashing. U = 1.69 m·s^{-1}, D = 3.9 mm, We = 513, Re = 1080, and Bo = 6.8×10^{-2}. (b) Symmetry-broken splashing. U = 2.15 m·s^{-1}, D = 3.74 mm, We = 732, Re = 1210, and Bo = 5.3×10^{-2}.

region as shown in **Fig. 10**. Such a thickness δ can be estimated as the order of $\delta \sim D\sqrt{U\mu_g/\sigma}$ (μ_g denotes viscosity of gas). For the present experiments, the value of δ is ranged from 20 to 200μm. The deformation of the layer is more pliant, because it has a smaller curvature than that of the droplet. The air gap pressure in the dimple region keeps the interfaces from touching. If the velocity reduction of the droplet is sustained until its sign changes, the droplet bounces. The time taken for the bouncing, which is estimated by Gopinath & Koch [11], was reasonable for the experimental results obtained by Jayaratne & Mason [24].

Next, let us consider the effect of gravity on the bouncing. In our experiments, the droplet diameter D, which ranges from 2.1 to 3.8 mm, is larger than capillary length L_c, which is estimated as 1.5 mm for silicone oil. Therefore gravity is not negligible in the surface deformation. This is also understood from **Fig. 7**, where the Bond number is larger than unity for 1 G cases. As shown in **Fig. 10**, during the approach of the droplet to the layer, deformation of the layer is suppressed by the surface tension (Laplace pressure) and also by gravity leveling. As described in Sec. 2, the time constant for the gravity leveling can be estimated as $\tau = \nu\lambda^2/(gH^3)$, where λ denotes the lateral length scale of the deformation. Here, λ can be roughly regarded as the droplet size D. Using the average values listed in **Table 2**, the time constant can be estimated as $\tau \approx 5$ ms, which is comparable to the time scale for the droplet impact. In contrast, the layer can deform comparatively more under low-gravity conditions due to an absence of gravity leveling. This feature may contribute to forming and maintaining the dimple region, which allows the bouncing of droplets even for higher impact velocities. **Figure 7** shows that bounces may occur for large Weber numbers when Bond numbers are small.

Another interest of our experiments is the effect of gravity on the occurrence of non-axisymmetric splashes. As mentioned above in Sec. 1, the threshold condition for the occurrence of symmetry-breaking has been investigated by Deegan et al. [10] in the plane of the Weber and the Reynolds numbers. In their experiments, the droplet impact shows non-axisymmetric splashes when the condition $We \cdot Re^{1/2} > 2.6 \times 10^4$ is satisfied. Their threshold is shown in **Fig. 9** as a dashed line, together with our experimental results. As described in Sec. 3, two groups of $m = 0$ (open) and $m > 0$ (filled) can be roughly divided by the line proposed by Deegan et al. [10]. It can be noted that the boundary of regions for $m = 0$ and $m > 0$ does not show a significant dif-

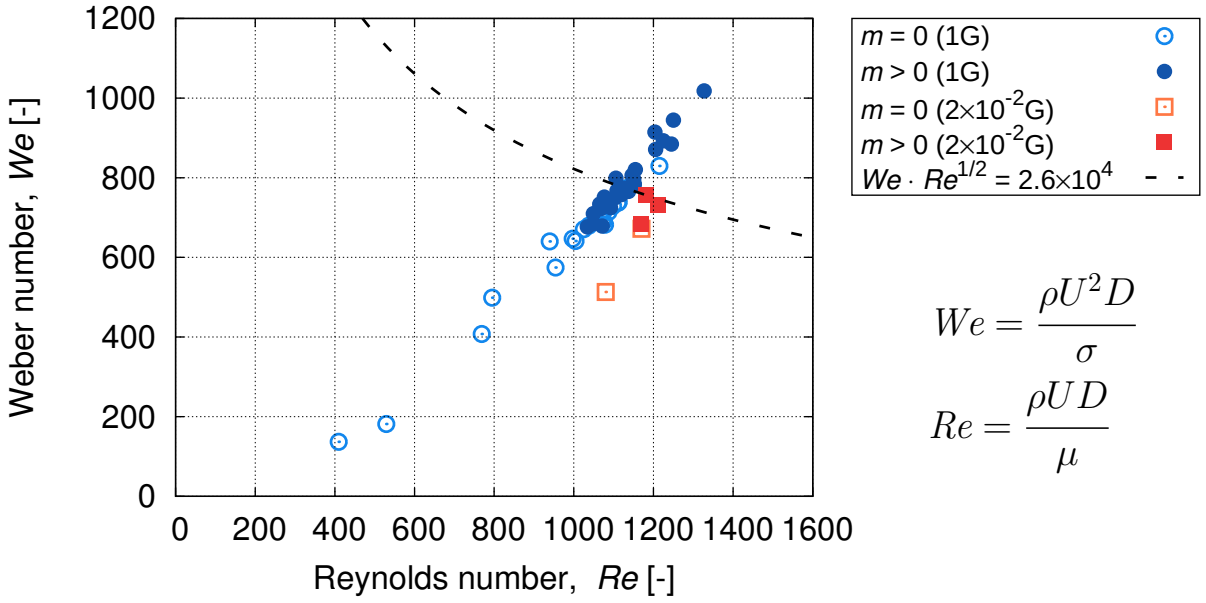

Fig. 9 The Reynolds and Weber numbers of droplet impacts. ○ and □ stand for axisymmetric ($m = 0$) splashes, whereas ● and ■ stand for non-axisymmetric ($m > 0$) splashes. The dashed line is the threshold with/without crown splash suggested by Deegan et al.[10].

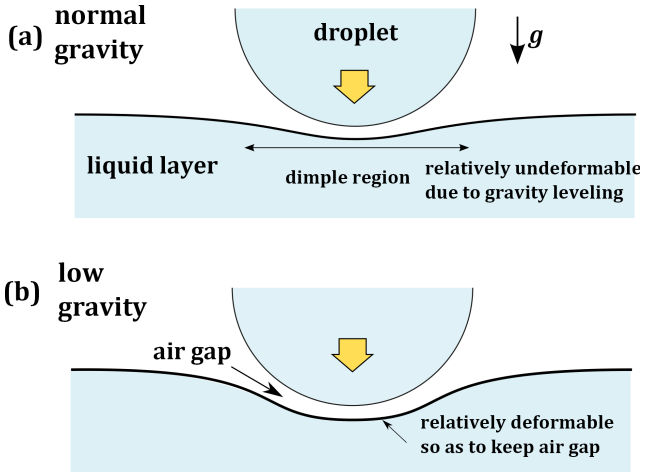

Fig. 10 A model for droplet bouncing.

ference regardless of the gravitational condition. This suggests that the instability mechanism for the appearance of the symmetry breaking does not depend on the gravity. Furthermore, the gravity-independence of this instability is also stated, in light of the fact that this instability is arising on the rim of the growing liquid sheet, whose length scale is much smaller than the capillary length. Zhang et al.[21] concluded that the symmetry-breaking is caused by the Rayleigh-Plateau instability, because the measured wavelength of the splashes showed a good agreement with those estimated based on the Rayleigh-Plateau instability mechanism, whereas those estimated based on the Rayleigh-Taylor type are much too larger than those of experiments. Our experiments support their conclusion from another perspective, that is, because the fact that secondary droplets are also observed under microgravity conditions, any gravity-dependent instability is contradicted by the essence of the symmetry-breaking of splashes.

5. Concluding remarks

Fluid motions after the impact of the droplet on the liquid layer were observed under various gravitational levels, ranging from 2×10^{-2} to 1 G for the first time. Whether the droplet bounces or splashes was found to be dependent not only on the Weber number but also on the Bond number. The droplet bouncing may occur with a larger Weber number when the Bond number is small. We have established that bouncing is likely to occur under low-gravity, since the liquid surface of the droplet and the liquid film become easy to deform due to the absence of the gravity-induced leveling effect. The symmetry-breaking of the growing liquid column, which may cause a breakup to secondary droplets, was observed with changing gravity. The threshold for the appearance of the instability is not affected by gravity. Our experiments suggest that the mechanism of this instability may be attributed to a type of gravity-independence, because it has been observed even under microgravity conditions.

Acknowledgments

This work was assisted by ground-based research activities supported by the Japan Space Forum under the guidance of JAXA. The authors thank Capt. D. Kageyama, S. Wakiya, R. Kitahara, and the other members staff of Diamond Air Service Inc. for carrying out the parabolic flight experiments. Thanks

are also given for K. Watari, T. Hayashi and V. Kumar the former students of Tokyo Metropolitan University for performing microgravity experiments. T. H. thanks Prof. A. Umemura of Nagoya University and Prof. A. Matsuo of Keio University for enlightening discussion on instability at the rim of lamella.

References

1) A. T. Mattick and A. Hertzberb: J. Energy, **5** (1981) 387.
2) D. B. van Dam and C. L. Clerc: Phys. Fluids, (2004) 3403.
3) L. Andreassi, V. Rocco, S. Ubertini and L. Allocca: In CNR 8th International Conference on Engines for Automobiles Technical Papers, 2007-24-0022, 2007.
4) A. M. Worthington: Proc. Royal Soc. London, **25** (1876) 261.
5) A. M. Worthington: Proc. Royal Soc. London, **25** (1876) 498.
6) A. L. Yarin: Annu. Rev. Fluid. Mech., **38** (2006) 159.
7) T. Tagawa: ISIJ International, **45** (2005)(7) 954.
8) H. Li, S. Mei, L. Gao and J. Liu: Int. J. Heat. Fluid Flow, **47** (2014) 1.
9) M. Rein: Fluid Dynamics Research, **12** (1993) 61.
10) R. D. Deegan, P. Brunet and J. Eggers: Nonlinearity, **21** (2008) C1.
11) A. Gopinath and D. L. Koch: Phys. Fluids, **13** (2001)(12) 3526.
12) T. Tran, H. de Maleprade, C. Sun and D. Lohse: J. Fluid Mech., **726** (2013)(R3) 1.
13) S. T. Thoroddsen, M. R.-J. Thoraval, K. Takehara and T. G. Etoh: J. Fluid Mech., **708** (2012) 469.
14) J. Zou, Y. Ren, C. Ji, X. Ruan and X. Fu: Exp. Therm. Fluld Sci., **51** (2013) 332.
15) J. Moláček and J. W. M. Bush: J. Fluid Mech., **727** (2013) 582.
16) L. V. Zhang, J. Toole, K. Fezzaa and R. D. Deegan: J. Fluid Mech., **703** (2012) 402.
17) G. Agbaglah and R. D. Deegan: J. Fluid Mech., **752** (2014) 485.
18) D. H. Peregrine: J. Fluid Mech., **106** (1981) 59.
19) Y. Zhang, K. Shimada, J. Nakagawa and T. Yabe: In 14th Symposium of the Japan Society of Computational Fluid Dynamics, A05-2, 2000.
20) M. Rieber and A. Frohn: Int. J. Heat Fluid, **20** (1999) 455.
21) L. V. Zhang, P. Brunet, J. Eggers and R. D. Deegan: Phys. Fluids, **22** (2010)(122105) 1.
22) D. Pettit: Saturday Morning Science: (2003).
23) Shin-Etsu Chemical Co. Ltd.: KF-96 Performance Test Results: (2014).
24) O. W. Jayaratne and B. J. Mason: Proc. Royal Soc. London, **Ser. A 280** (1964) 545.